Nonlinear Optical Properties of 2D Quantum Materials

ExpandQISE Track 2: Quantum Materials Institute: 2D Materials, heterostructures and metasurfaces for quantum light

Arik Ahmed[1,3,4], Himal Oli[3,4,5], J. Pierce Fix[2,3], Sheikh Parvez[2,3], Jane Peabody[2,3,6], Ilya Mikhailov[7], Venera Alimova[7]
Nicholas J. Borys[2,3,4,6], Alexey Lipatov[1,4,7], Tula Paudel[4,5], Shan Zhou[1,3,4], Steve Smith[1,3,4]
[1]Nanoscience & Biomedical Engineering, South Dakota School of Mines and Technology
[2]Department of Physics, Montana State University
[3]MonArk Quantum Foundry (Montana State & University of Arkansas, San Diego State, South Dakota Mines, University of Utah)
[4]Quantum Materials Institute (South Dakota Mines & University of Utah)
[5]Department of Physics, South Dakota Mines
[6]University of Utah
[7]Department of Chemistry, Biology and Health Sciences, South Dakota Mines

Quantum Information Science

Quantum Information Science (QIS) encompasses efforts to develop quantum computers, quantum sensors, and secure communications networks, all of which obtain some advantage over their classical counterparts due to the intrinsic properties of quantum mechanics. A leading effort towards secure communications involves the exchange of cryptographic keys using a quantum network, so called quantum key distribution (QKD) systems. Leading efforts to realize QKD systems involve photonics and nanophotonics which are the focus of this talk.

Quantum Computing[1]	Quantum Communications[2]	Quantum Sensing[3]

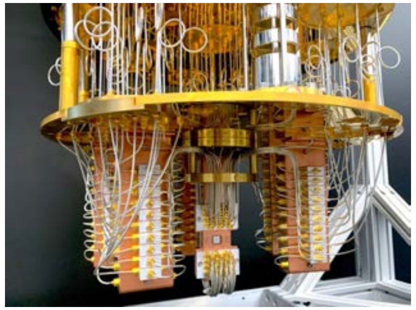

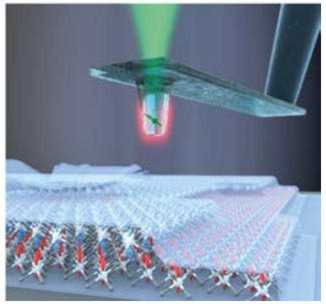

[1]https://www.popsci.com/technology/in-photos-journey-to-the-center-of-a-quantum-computer/

[2]https://thequantuminsider.com/2023/02/20/quantum-entanglement-communication/

[3]https://quantum-sensing.physik.unibas.ch/en/p/461/6/

Superposition and Entanglement

QIS is based on two important features of quantum mechanics, superposition and entanglement:

Superposition[1]

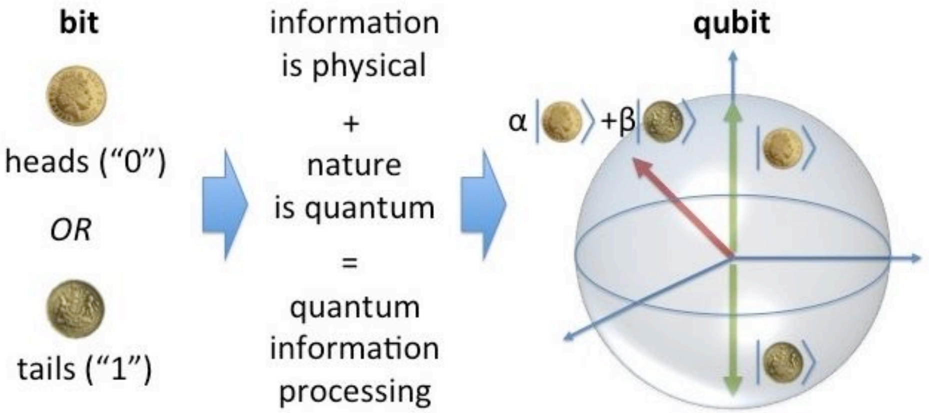

Information is encoded in a superposition of states, for a two-level system this is termed a qubit.

Entanglement[2]

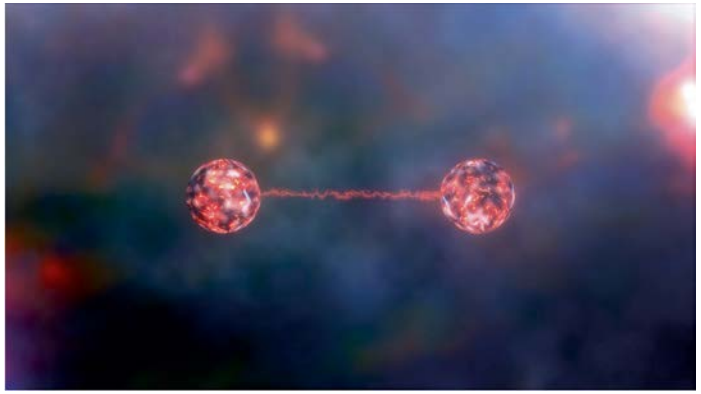

Pioneering quantum information science

4 October 2022, the Royal Swedish Academy of Sciences announced that the 2022 Nobel Prize in Physics would be awarded to three scientists — Alain Aspect, John F. Clauser and Anton Zeilinger — "for experiments with entangled photons, establishing the violation of Bell inequalities and pioneering quantum information science."

[1]https://cnqo.phys.strath.ac.uk/research/quantum-information/

[2]*Nature Computational Science* 2022 Vol. 2 Issue 11 Pages 687-688
DOI: 10.1038/s43588-022-00368-0

EPR Paradox and Bells Theorem

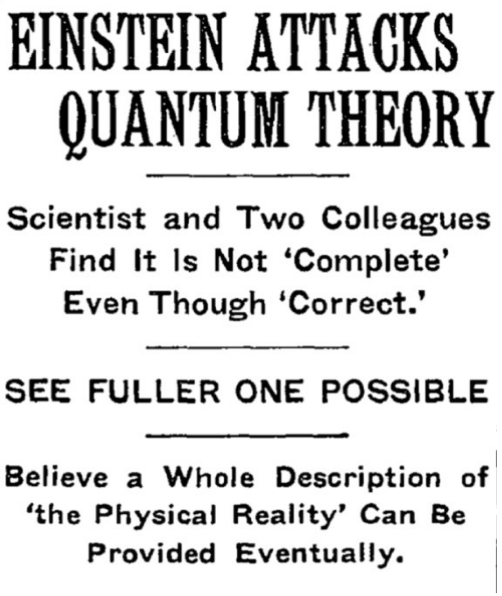
EINSTEIN ATTACKS QUANTUM THEORY

Scientist and Two Colleagues Find It Is Not 'Complete' Even Though 'Correct.'

SEE FULLER ONE POSSIBLE

Believe a Whole Description of 'the Physical Reality' Can Be Provided Eventually.

New York Times, May 4, 1935

EPR Parodox[1]

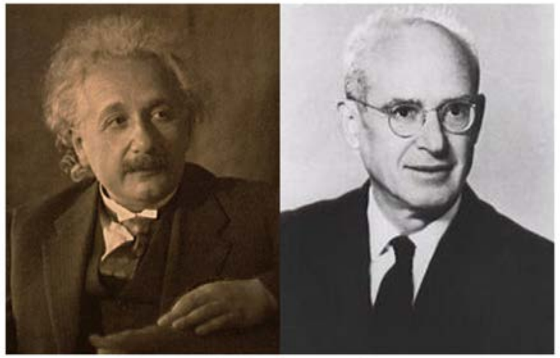

Einstein and Rosen drafted in coordination with Podolsky their famous paper labeling effects originating from complementarity and entanglement the Einstein-Podolsky-Rosen paradox. – Wikipedia

"EPR appeared to have contrived a means to establish the exact values of *either* the momentum *or* the position of B due to measurements made on particle A, without the slightest possibility of particle B being physically disturbed."

[1]https://en.wikipedia.org/wiki/Einstein–Podolsky–Rosen_paradox

Bells Theorem[2]

Locality

"… that the result of a measurement on one system be unaffected by operations on a distant system…" (Bell)

John Stewart Bell is the originator of Bell's theorem, important in quantum physics regarding hidden variable theories. – Wikipedia

- In 1964 John Stewart Bell replied on the Einstein-Podolsky-Rosen Paradox, deriving an inequality making it possible to distinguish between all local realistic theories and quantum theory.
- in the early 80's Aspect, Grangier and Roger showed their experimental data violated the inequality, refuting all local realistic theories and proving that quantum theory was right!

[2]http://www.qutools.com

Entangled Photons by SPDC on a Global Scale

Satellite-based entanglement over 1200 kilometers[2]

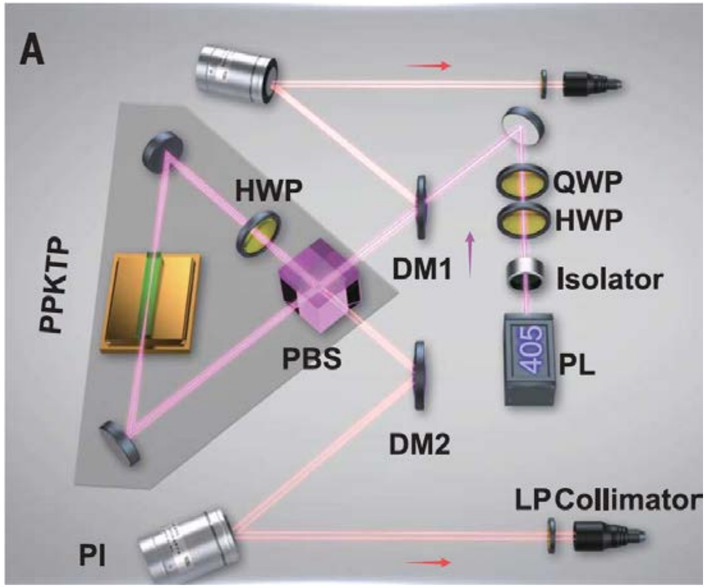

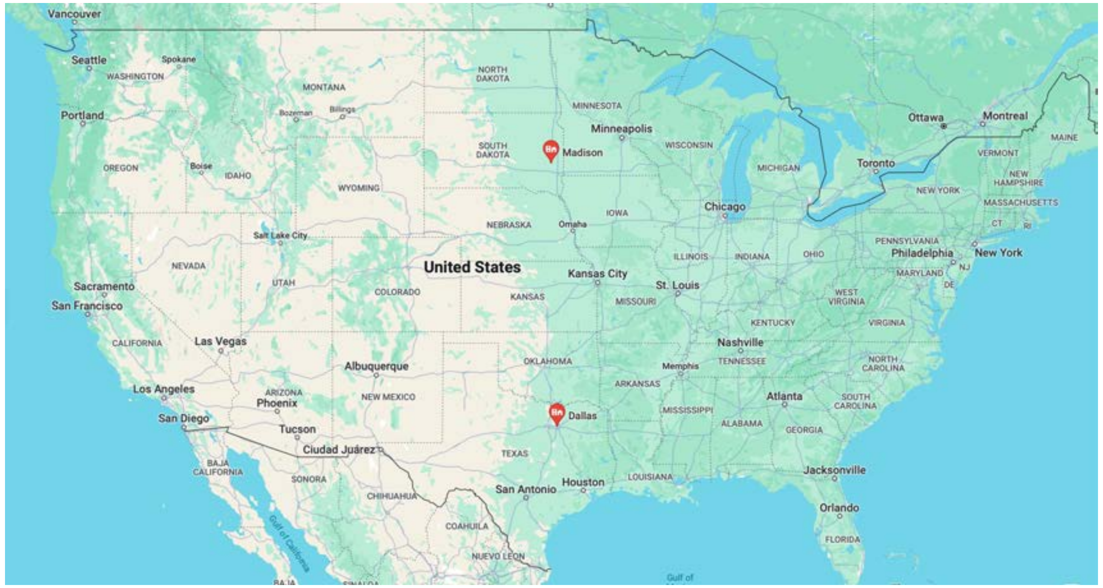

Entanglement over global length scales demonstrated via entangled photons generated by spontaneous parametric downconversion (SPDC) transmitted via satellite.

[2]J. Yin, Y. Cao, Y.-H. Li, S.-K. Liao, L. Zhang, J.-G. Ren, et al. *Science* 2017 Vol. 356 Pages 1140-1144
DOI:10.1126/science.aan3211

2D Materials for Integrated Quantum Technologies

Motivation: Parametric downconverters, single photon emitters and detectors are key components of quantum information systems. Structure-property relations of the materials they comprise determine performance and guide their development and application.

Focus: Develop spatially- and spectrally-resolved multiphoton imaging methods to characterize quantum materials on passive and enhancing substrates, including metasurfaces.

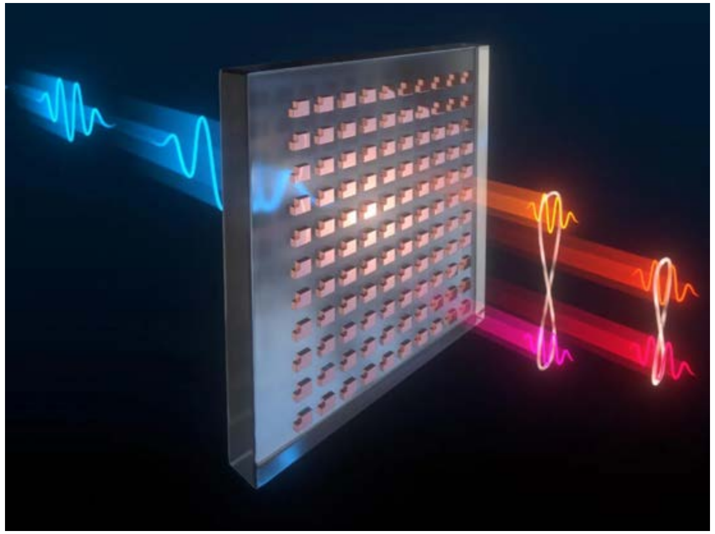

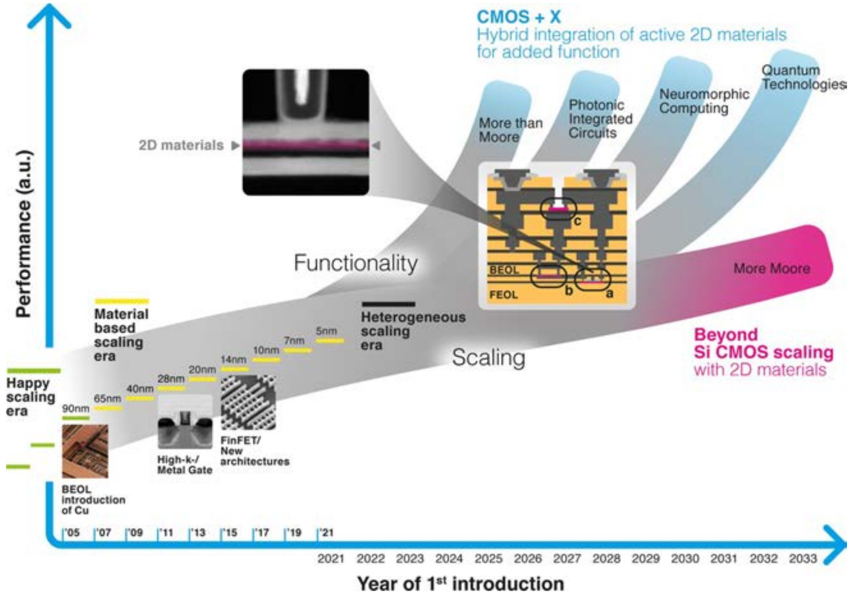

Parametric down conversion generates entangled photon pairs[1] for quantum communications. 2D materials can integrate into CMOS fab, promising properties[2].

[1]https://spectrum.ieee.org/metasurface-entangled-photons

[2]Lemme, M.C., Akinwande, D., Huyghebaert, C. *et al.* 2D materials for future heterogeneous electronics. *Nat Commun* **13**, 1392 (2022). https://doi.org/10.1038/s41467-022-29001-4

⇒ Parametric downconversion

⇒ $\chi^{(2)}_{ijk}$ in 2D heterostructures

⇒ Integrable with chip scale fab

Nonlinear Optics, 2D Materials and Metaphotonics

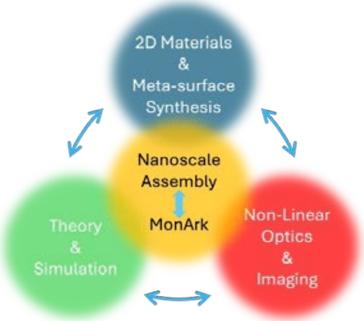

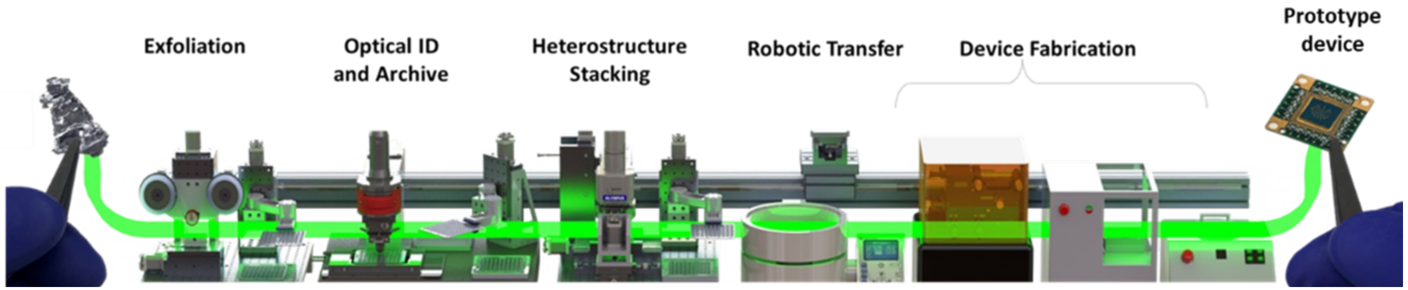

Methods Available at South Dakota Mines: Nonlinear imaging, synthesis of 2D materials and self-assembled nanostructures/metasurfaces, FDTD simulations and density functional theory.

MonArk Enabling Infrastructure: The 2D-QMaPs of the MonArk NSF Quantum Foundry are a primary resource for the preparation of 2D samples from bulk crystals, assembly of 2D heterostructures of multiple 2D layers, and the fabrication of prototype quantum devices.

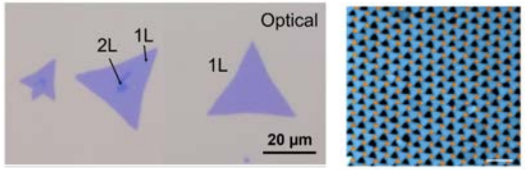

South Dakota Mines team: Expand scope to include materials synthesis and theory to explore limits of $\chi^{(2)}_{ijk}$ in 2D materials and 2D materials integrated with metasurfaces.

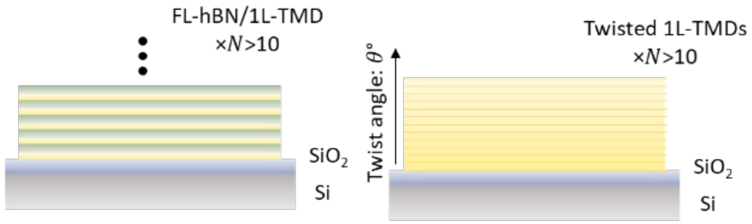

MonArk team: Collaborate on the development of multilayer 2D materials heterostructures and varying interlayer coupling leading to optimal $\chi^{(2)}_{ijk}$.

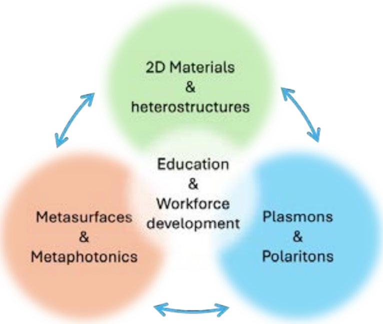

Scientific Scope

⇒ materials, growth, theory and optics ⇒ MonArk 2D-QMaP, heterostructures ⇒ metaphotonics, polaritons, plasmons

Spectrally-Resolved Multi-photon Imaging and Spectroscopy

Quantum Materials Institute

MonArk Quantum Foundry

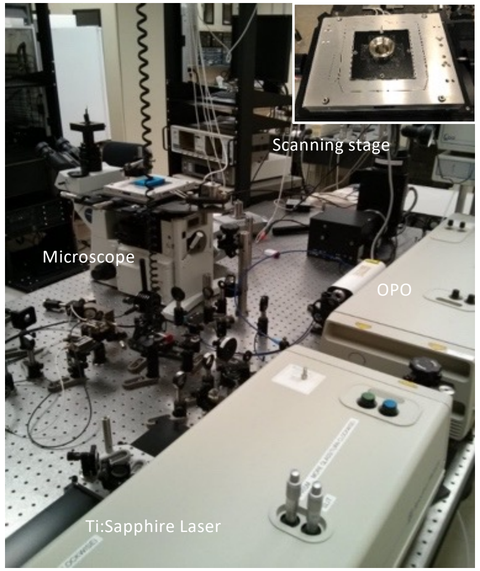

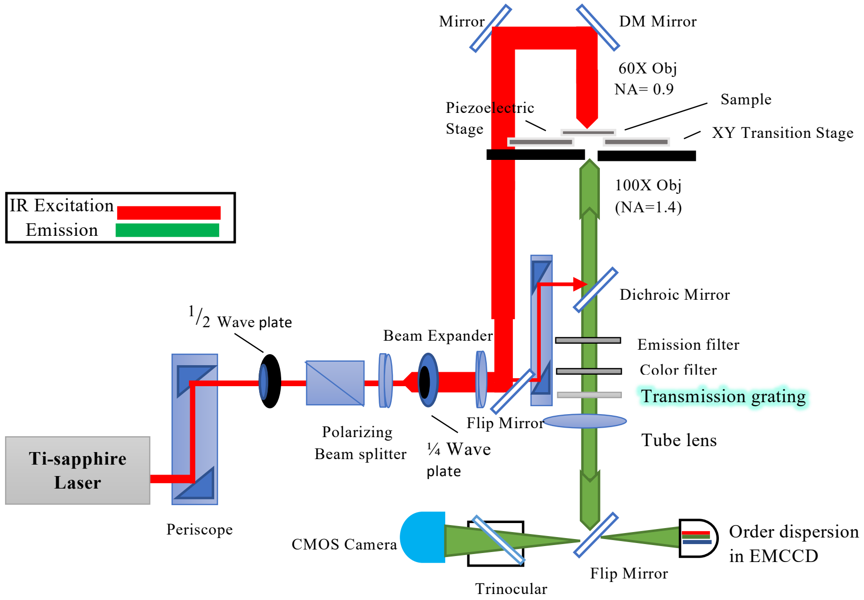

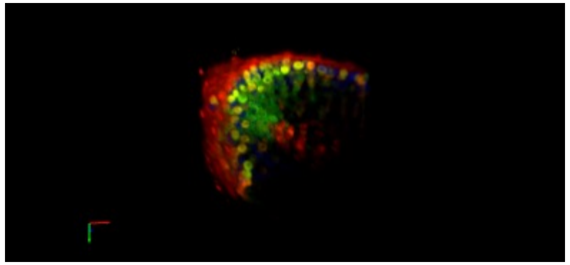

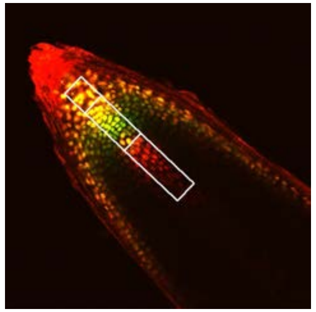

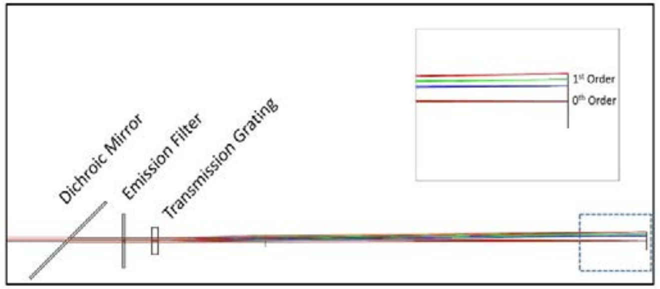

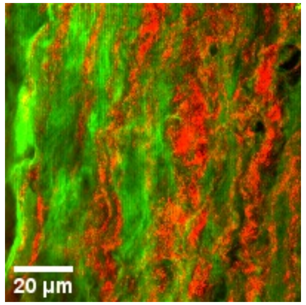

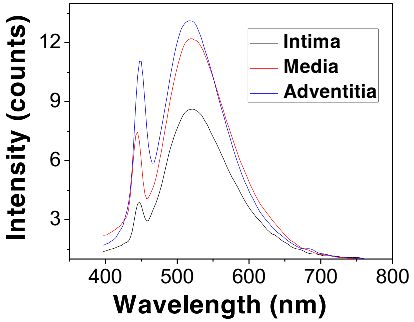

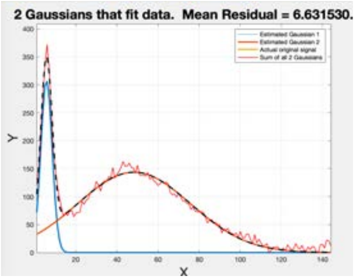

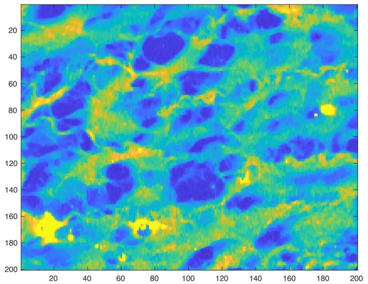

Figure: (left): Spectrally-resolved multiphoton microscope at SDSMT, with femtosecond lasers and scanning stage. (right): Schematic diagram and example multiphoton fluorescence (green) and SHG (red) image and spectra (SHG at 450nm) of collagen in arterial wall. Upper right: animation of 3D multiphoton excited fluorescence from transgenic plant (animation and maximum intensity projection). Lower right: deconvolved arterial wall image.

⇒ Imaging point spread function (x,y) ⇒ Spectra resolved, measure scattering ⇒ Normalize out intensity variations

Multiphoton spectrally-resolved Imaging of WSe_2 (Borys)

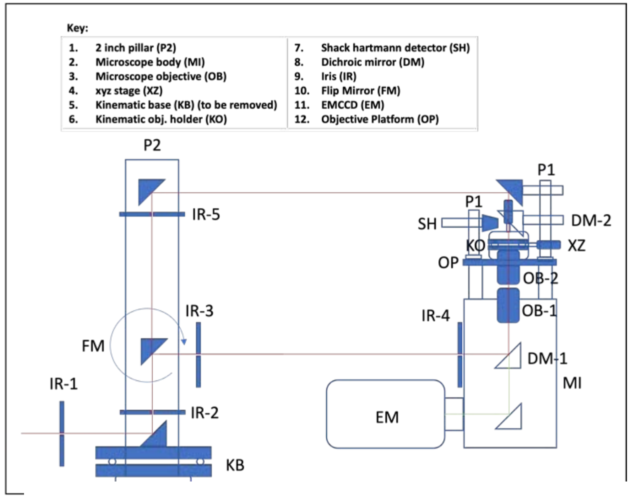

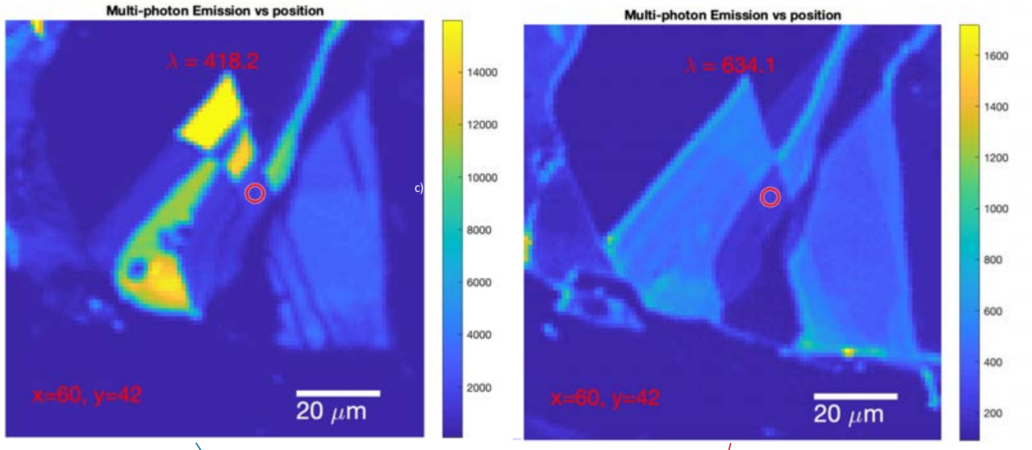

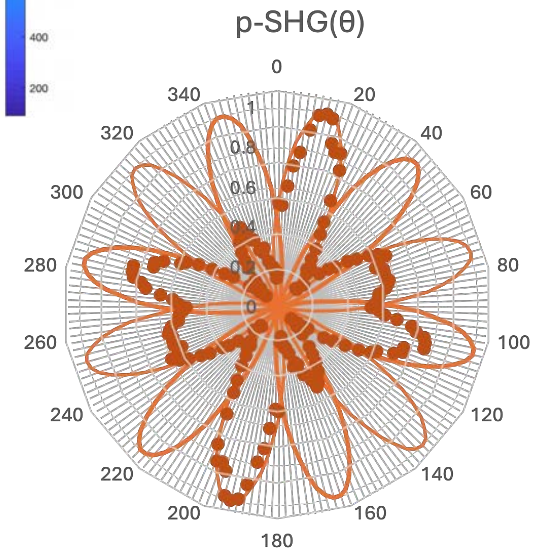

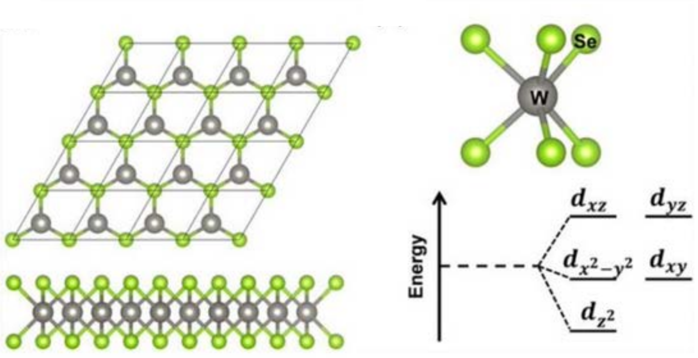

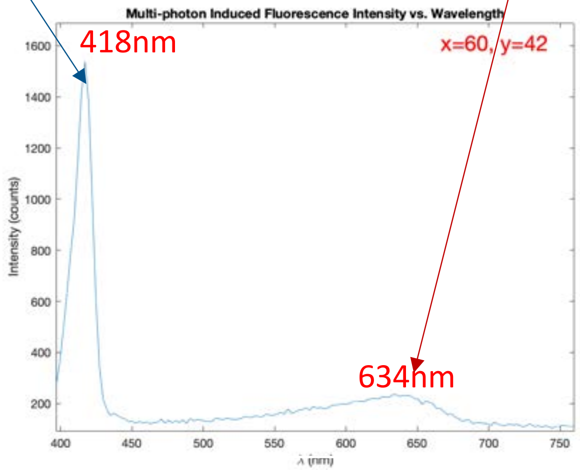

⇒ SHG indicates monolayer fluctuations ⇒ Correlated MPL details layers ⇒ Spectra, Polarization at each point.

Angle-resolved linearly-polarized SHG from WSe_2 few-layer stacks

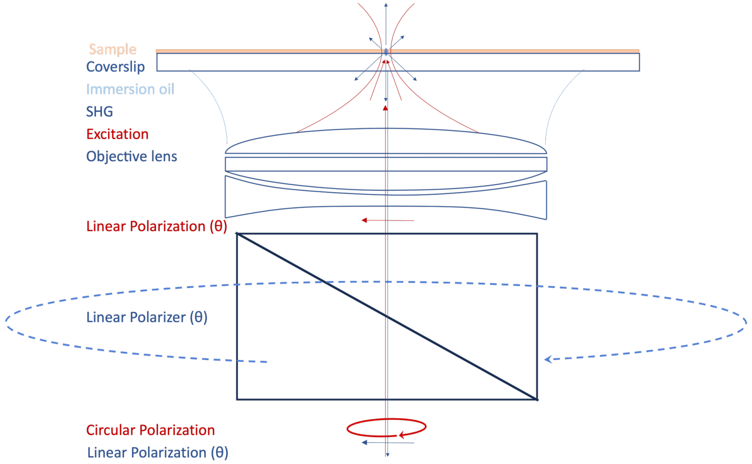

Angle resolved SHG

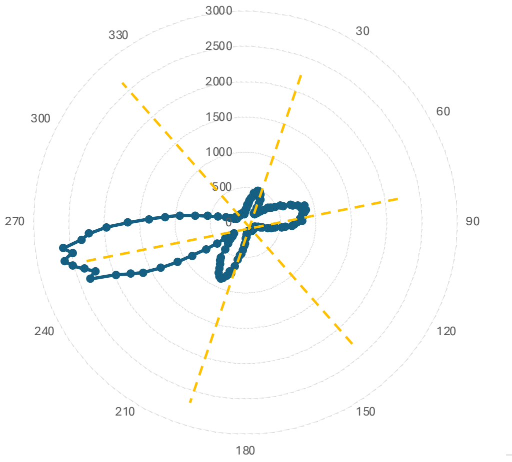

Corrected SHG

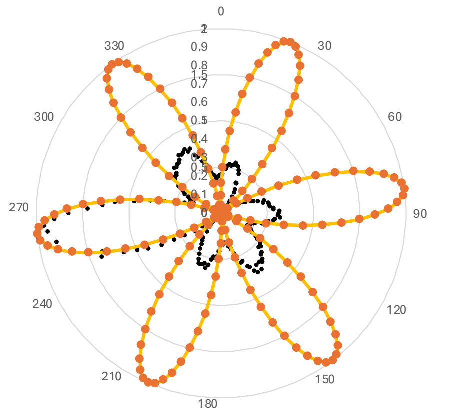

Spectrally-integrated SHG

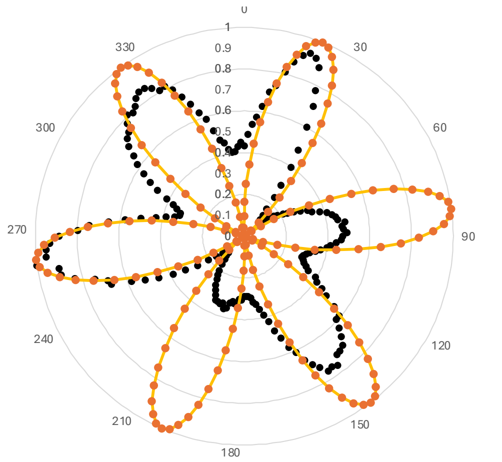

White light @ 100X

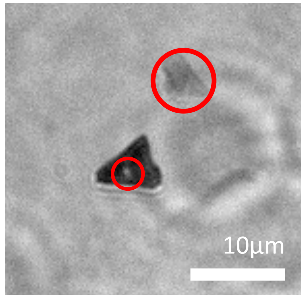

Dependence of Power after λ/4 plate compared to average

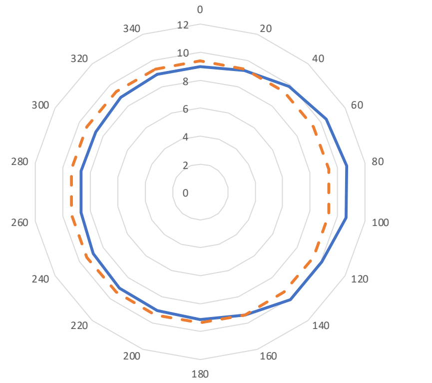

Dye Sphere SUM(C306:326)

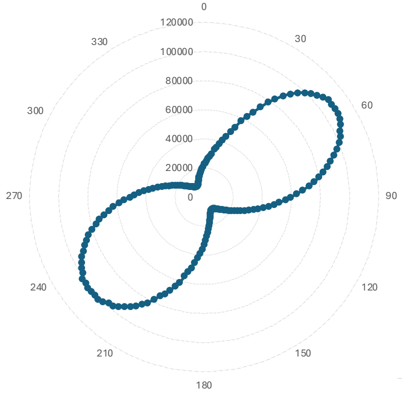

Corrected SHG

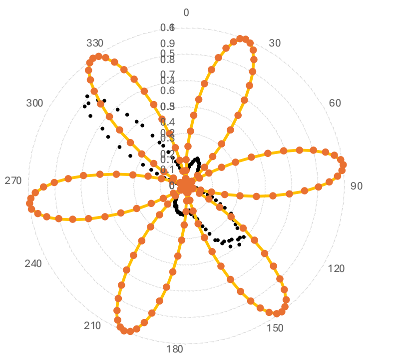

Spectrally-integrated SHG

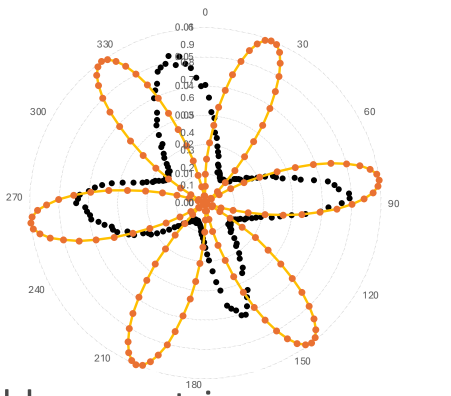

⇒ circularly polarized light input

⇒ primarily multi-layer samples

⇒ 6-fold and 4-fold symmetries appear

Correcting ellipticity in dichroic mirror to obtain circular polarization

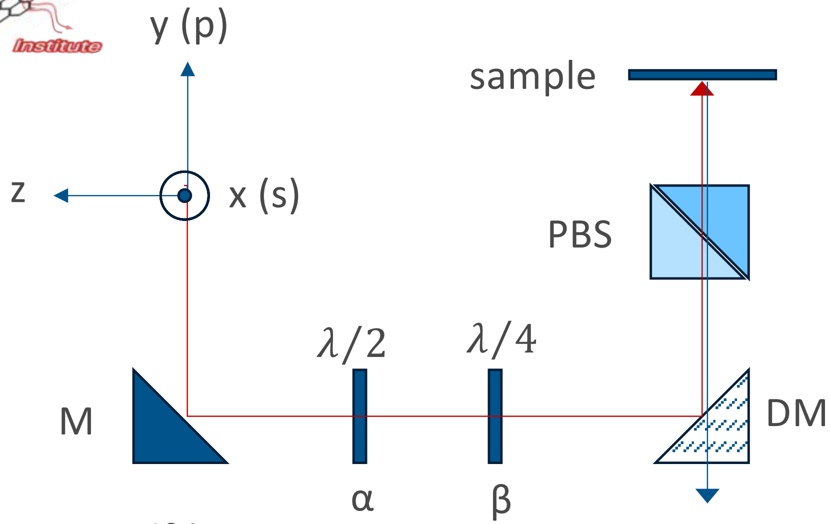

Jones matrices for system elements:

$$\underline{\mathbf{M}}_\delta = \begin{pmatrix} R_s e^{i\delta/2} & 0 \\ 0 & R_p e^{-i\delta/2} \end{pmatrix} \qquad \underline{\mathbf{R}} = \begin{pmatrix} \cos\theta & -\sin\theta \\ \sin\theta & \cos\theta \end{pmatrix}$$

$$\mathbf{v}_{in} = \begin{pmatrix} 0 \\ 1 \end{pmatrix} \qquad \underline{\mathbf{M}}_{\lambda/2} = \begin{pmatrix} i & 0 \\ 0 & -i \end{pmatrix} \qquad \underline{\mathbf{M}}_{\lambda/4} = \begin{pmatrix} e^{i\pi/4} & 0 \\ 0 & e^{-i\pi/4} \end{pmatrix}$$

$$\underline{\mathbf{M}}_\theta = \underline{\mathbf{R}}^{-1}(\theta)\, \underline{\mathbf{M}}_{\lambda/n}\, \underline{\mathbf{R}}(\theta) \qquad \mathbf{v}_{out} = \underline{\mathbf{M}}_{sys} \begin{pmatrix} 1 \\ 0 \end{pmatrix}$$

$$\underline{\mathbf{M}}_{sys} = \begin{pmatrix} R_s e^{i\delta/2} & 0 \\ 0 & R_p e^{-i\delta/2} \end{pmatrix} \begin{pmatrix} \cos\beta & \sin\beta \\ -\sin\beta & \cos\beta \end{pmatrix} \begin{pmatrix} e^{i\pi/4} & 0 \\ 0 & e^{-i\pi/4} \end{pmatrix} \begin{pmatrix} \cos\beta & -\sin\beta \\ \sin\beta & \cos\beta \end{pmatrix} \begin{pmatrix} \cos\alpha & \sin\alpha \\ -\sin\alpha & \cos\alpha \end{pmatrix} \begin{pmatrix} i & 0 \\ 0 & -i \end{pmatrix} \begin{pmatrix} \cos\alpha & -\sin\alpha \\ \sin\alpha & \cos\alpha \end{pmatrix}$$

$$\mathbf{v}_{out} = e^{i\delta/2} \begin{pmatrix} e^{i\delta/2}\{(1+i)\cos 2\alpha - (1-\mathrm{i})\cos 2(\alpha-\beta)\}R_s \\ e^{-i\delta/2}\{(1+i)\sin 2\alpha + (1-i)\sin 2(\alpha-\beta)\}R_p \end{pmatrix}$$

$$\mathbf{v}_{out} = e^{i\delta/2} \begin{pmatrix} e^{i\delta/2}\{\cos 2\alpha - \cos 2(\alpha-\beta) + i(\cos 2\alpha + \cos 2(\alpha-\beta))\}R_s \\ e^{-i\delta/2}\{\sin 2\alpha + \sin 2(\alpha-\beta) + i(\sin 2\alpha - \sin 2(\alpha-\beta))\}R_p \end{pmatrix}$$

$$\delta \sim \pi/4 \qquad \mathbf{v}_{out} = \begin{pmatrix} \left(\frac{1}{2}+\frac{i}{2}\right)(-1)^{3/8} R_s(\cos 2\alpha + i\cos 2(\alpha-\beta)) \\ \left(\frac{1}{2}+\frac{i}{2}\right)(-1)^{1/8} R_p(\sin 2\alpha - i\sin 2(\alpha-\beta)) \end{pmatrix}$$

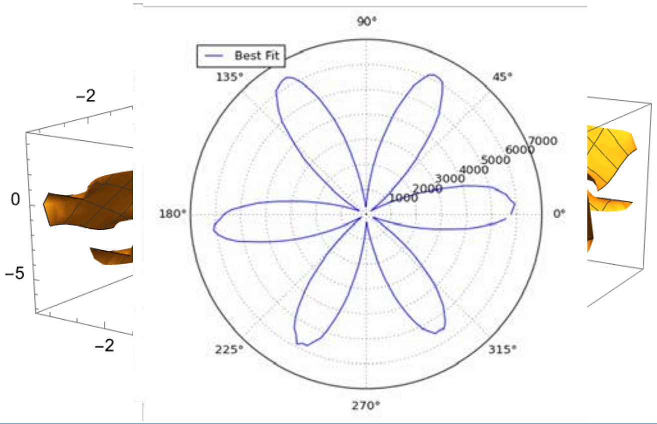

Expanding the palette of 2D Materials (Lipatov, Paudel)

ACS NANO

www.acsnano.org

Giant Modulation of Second-Harmonic Generation in $CuInP_2S_6$ by Interfacing with MoS_2 Atomic Layers

Dawei Li,* Xinyi Hou, Fanyi Kong, Kun Wang, and Xia Hong*

Cite This: ACS Nano 2024, 18, 32890–32898 Read Online

nature photonics

Article

https://doi.org/10.1038/s41566-024-01434-x

Giant optical nonlinearity of Fermi polarons in atomically thin semiconductors

Received: 21 September 2023

Accepted: 25 March 2024

Liuxin Gu[1,9], Lifu Zhang[1,9], Ruihao Ni[1], Ming Xie[2], Dominik S. Wild[3], Suji Park[4], Houk Jang[4], Takashi Taniguchi[5], Kenji Watanabe[6], Mohammad Hafezi[7] & You Zhou[1,8]

J A C S

JOURNAL OF THE AMERICAN CHEMICAL SOCIETY

Communication

Regulating Second-Harmonic Generation by Van der Waals Interactions in 2D Lead Halide Perovskite Nanosheets

Wen-Juan Wei, Xingxing Jiang, Li-Yuan Dong, Wei-Wei Liu, Xiao-Bo Han, Yan Qin, Kai Li, Wei Li, Zheshuai Lin, Xian-He Bu, and Pei-Xiang Lu

J. Am. Chem. Soc., Just Accepted Manuscript • DOI: 10.1021/jacs.9b01874 • Publication Date (Web): 26 May 2019

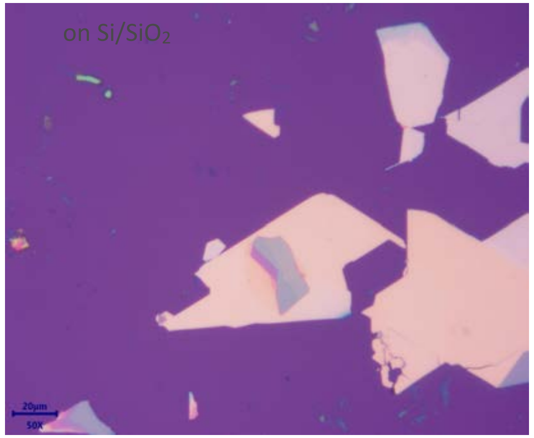

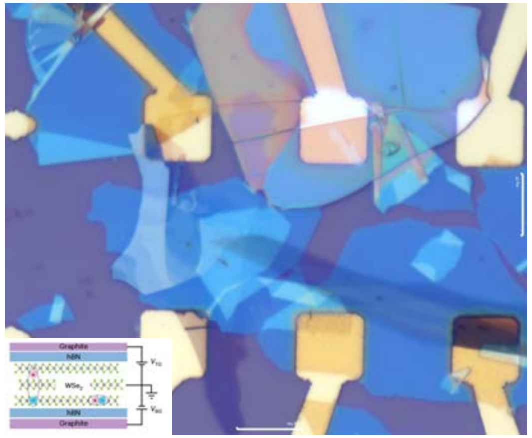

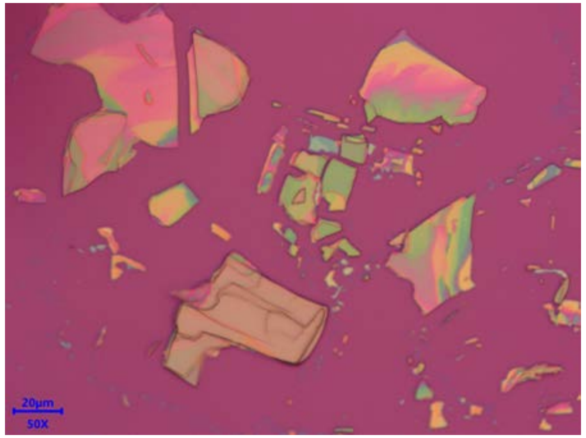

⇒ CIPS/MoS2 heterostructures

⇒ MonArk WSe_2/h-BN heterostrucures

⇒ Perovskite layered materials

2D non-centrosymmetric materials synthesis

MonArk
Quantum Foundry

Synthesis of 2D materials (α-In_2Se_3, β-In_2Se_3, CIPS)

CVT method

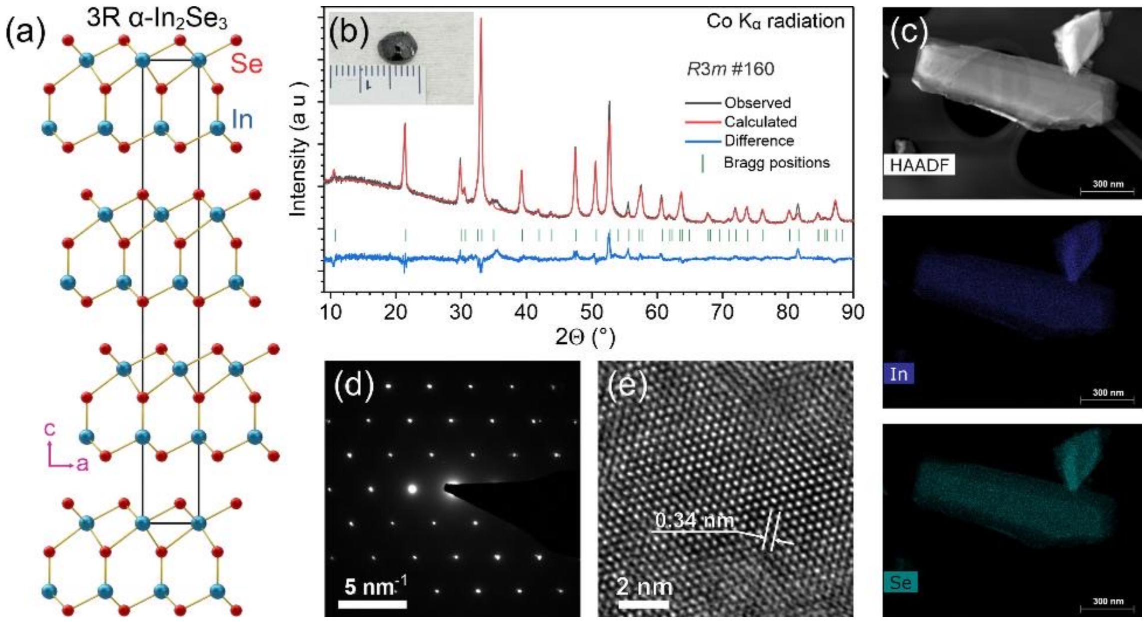

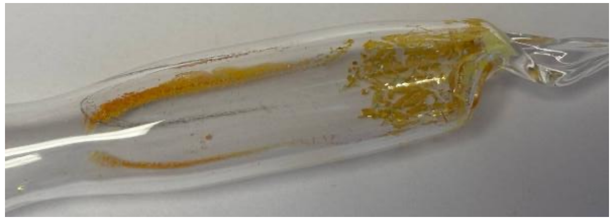

CIPS crystals in an ampoule

CVD method

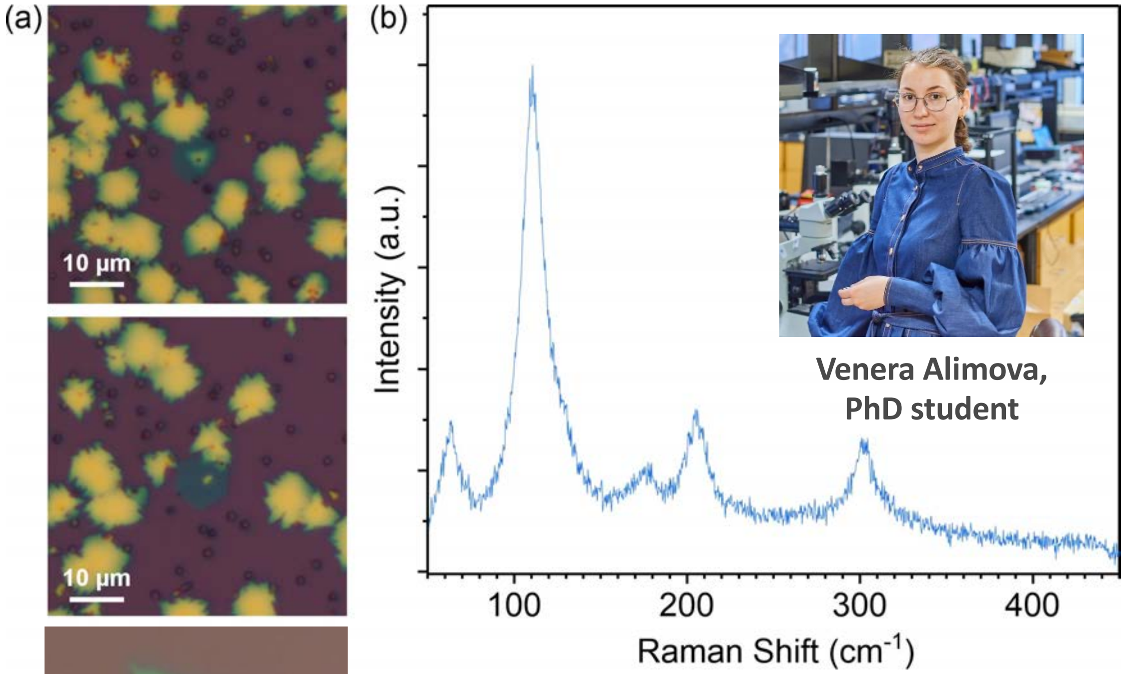

Venera Alimova, PhD student

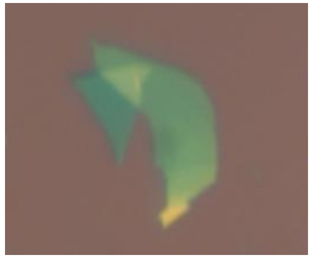

MoS_2/In_2Se_3 heterostructure

2D heterostructures and devices fabrication

MonArk Quantum Foundry

Photo of a flake transfer setup

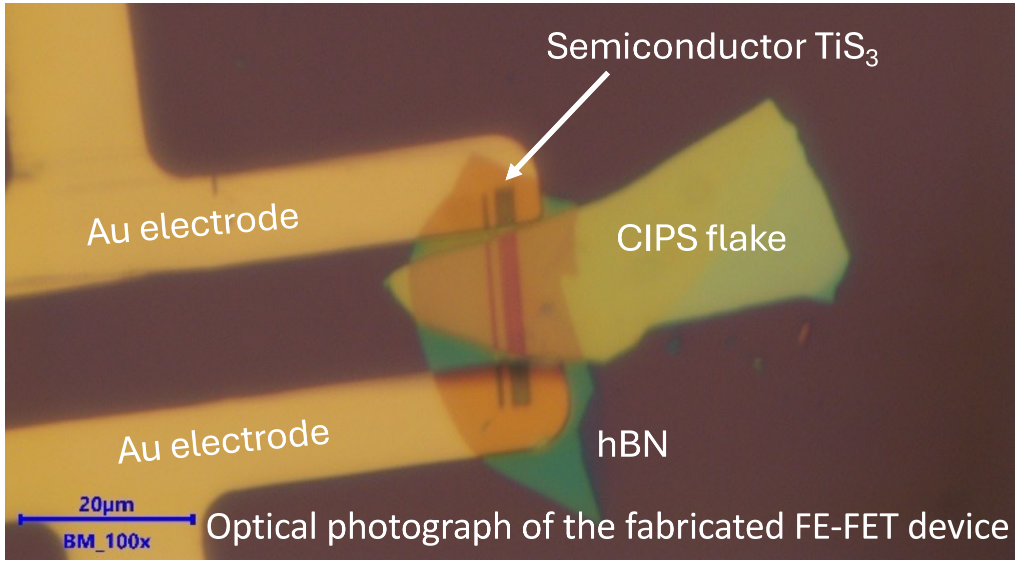

Optical photograph of the fabricated FE-FET device

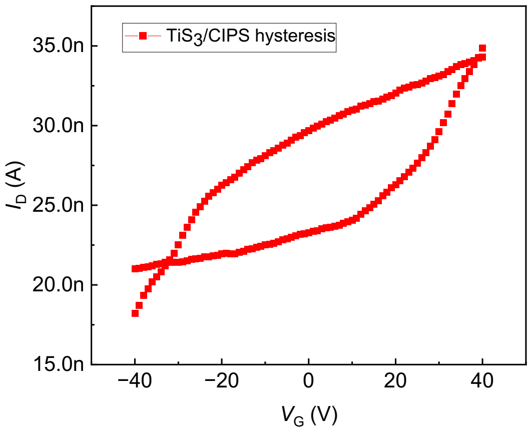

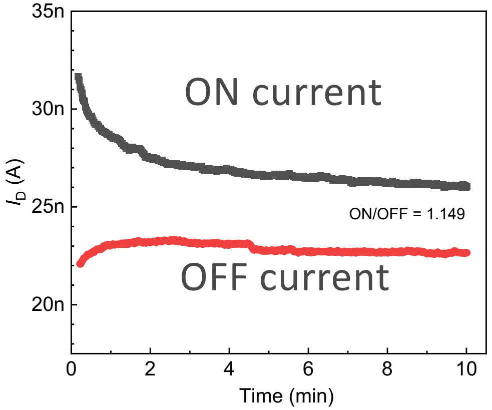

Ilya Mikhailov, PhD student

Multiphoton Imaging of In_2Se_3 (Lipatov)

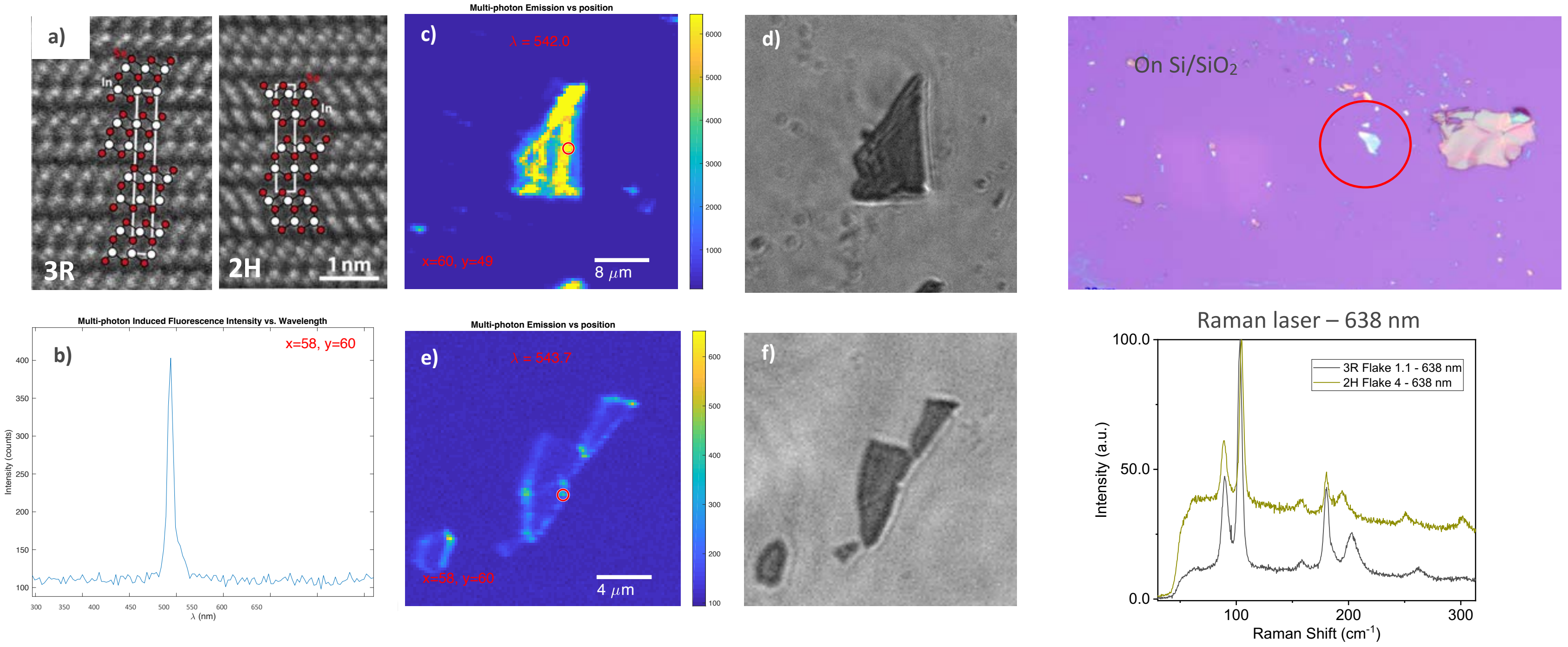

Figure 4: (a) High-resolution high-angle annular dark-field scanning transmission electron microscopy (HAADF-STEM) Z-contrast images of 2H and 3R In_2Se_3 together with the structural models[1]. **(b)** SHG spectrum of In_2Se_3 **(c)** Spatially resolved SHG from 2H stacked In_2Se_3 **(d)** White light image of 2H stacked In_2Se_3 **(e)** Spatially resolved SHG from 3R stacked In_2Se_3 **(f)** White light image of 3R stacked In_2Se_3

→ Predicted to have high $\chi^{(2)}_{ijk}$ and sensitivity to interlayer coupling

→ Variation in intensity observed, SHG (3R) 10X SHG (2H)

MonArk Quantum Foundry

Arik Ahmed

1. Küpers, M., Konze, P. M., Meledin, A., Mayer, J., Englert, U., Wuttig, M., & Dronskowski, R. (2018). Controlled crystal growth of indium selenide, In2Se3, and the crystal structures of α-In2Se3. Inorganic chemistry, 57(18), 11775-11781.

⇒ Imaged SHG in 3R and 2H In_2Se_3 ⇒ Edges highlighted, suppressed in 2H ⇒ Stacking determined by Raman

SHG Imaging in CIPS/MoS2 heterostructure (Lipatov)

Arik Ahmed

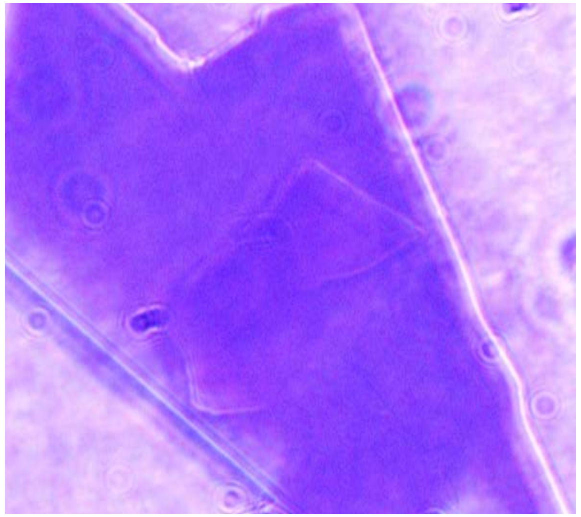

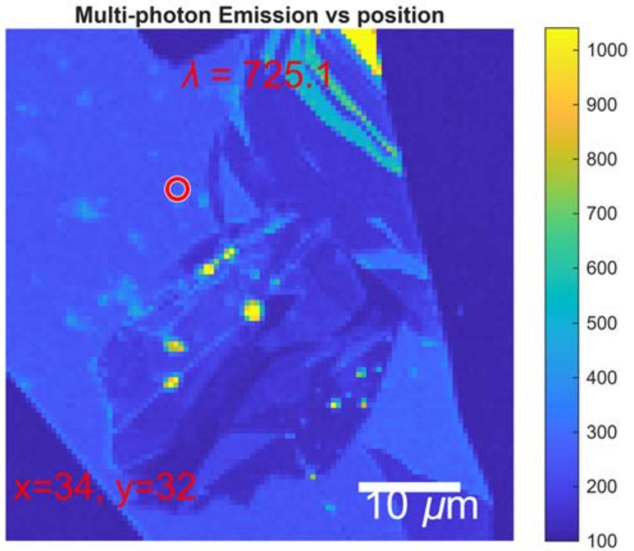

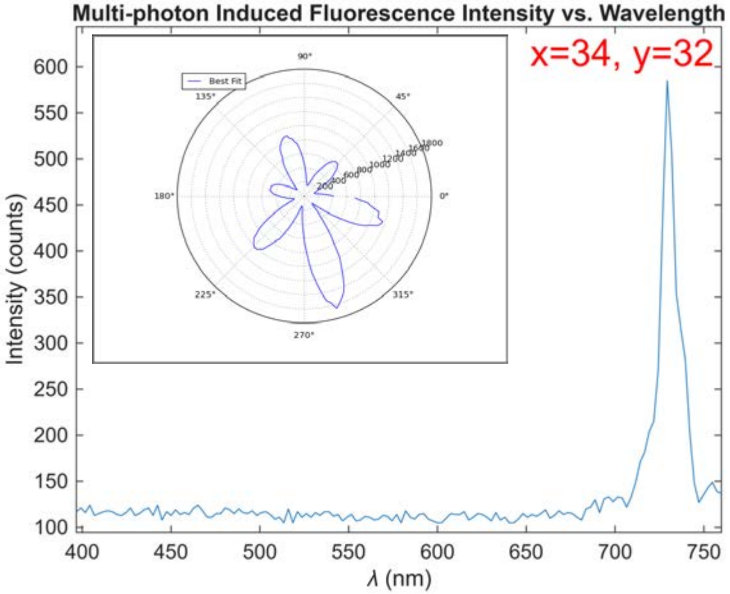

⇒ CIPS/MoS_2 widefield image

⇒ CIPS/MoS_2 SHG image

⇒ SHG spectra, and angular dependence

Polarized SHG in CIPS and fits

SHG intensity map

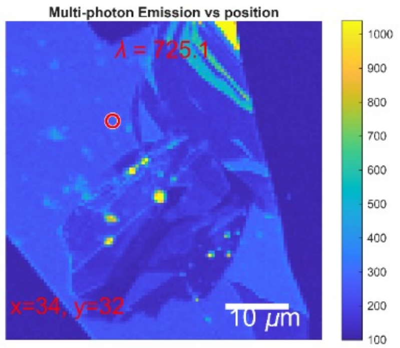

Region 1

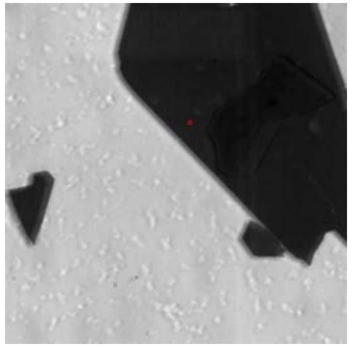

Region 2

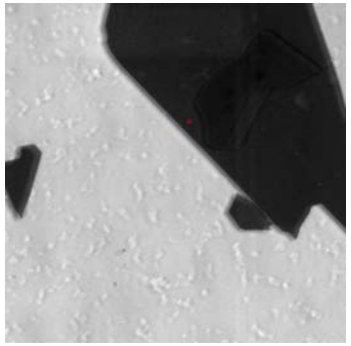

Region 3

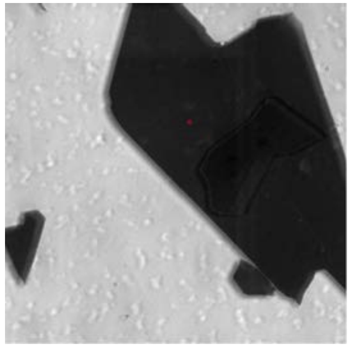

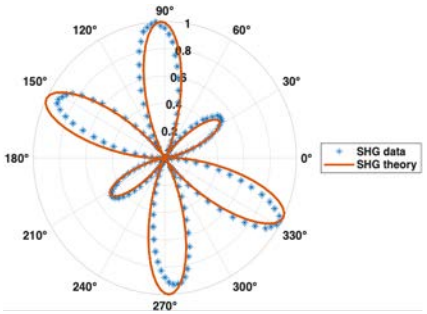

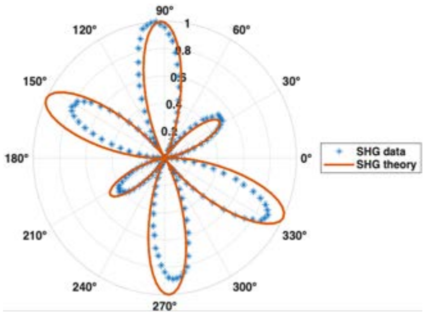

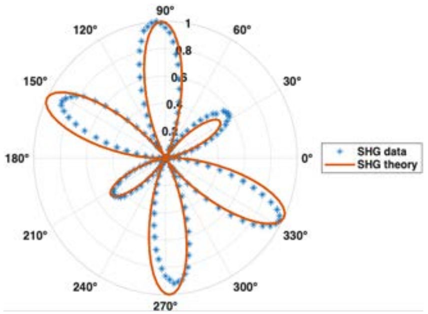

Putting new tensor elements into the formula above, we could get strain-dependent SHG intensity:

$$I_{\parallel}^{(C_{2v})} = \left|d_{22}^{(D_{3h})}(\cos 3\theta + \varepsilon_a(a_1\cos^3\theta - b_1\sin^2\theta\cos\theta - 2c_1\sin^2\theta\cos\theta))\right|^2$$
$$I_{\perp}^{(C_{2v})} = \left|d_{22}^{(D_{3h})}(\sin 3\theta + \varepsilon_a(a_1\sin\theta\cos^2\theta - b_1\sin^3\theta + 2c_1\sin\theta\cos^2\theta))\right|^2 \quad (6)$$

where θ is the included angle between unique armchair crystal orientation which remains a C_2 axis. Under ε_z, we would obtain the same formula shown above with ε_a, a_1, b_1, c_1 replaced by ε_z, a_2, b_2, c_2 respectively.

S9. Parameters used to characterize strain-dependent $\overleftrightarrow{d}$.

Table S1 | Parameters used to characterize strain magnitude

	a_i	b_i	c_i
$i = 1$	-0.31	-0.19	-0.17
$i = 2$	-0.12	-0.26	-0.25

Using the parallel I_{SHG} formula from the supp. info of Ref.1 and inputting the same a1, b1 and c1, an offset of 33 degrees, and an ϵ_a value of 1.5 (i.e. 1.5% strain). The formula assumes the strain is aligned with the armchair axis.

1. Liang, J., Zhang, J., Li, Z., Hong, H., Wang, J., Zhang, Z., ... & Yu, D. (2017). Monitoring local strain vector in atomic-layered MoSe2 by second-harmonic generation. *Nano letters*, *17*(12), 7539-7543.

Band structure of monolayer 2D $(Benzylammonium)_2PbBr_4$ Perovskite (Paudel)

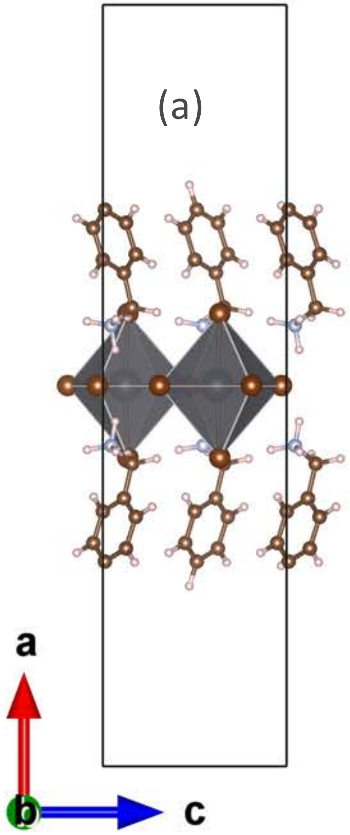

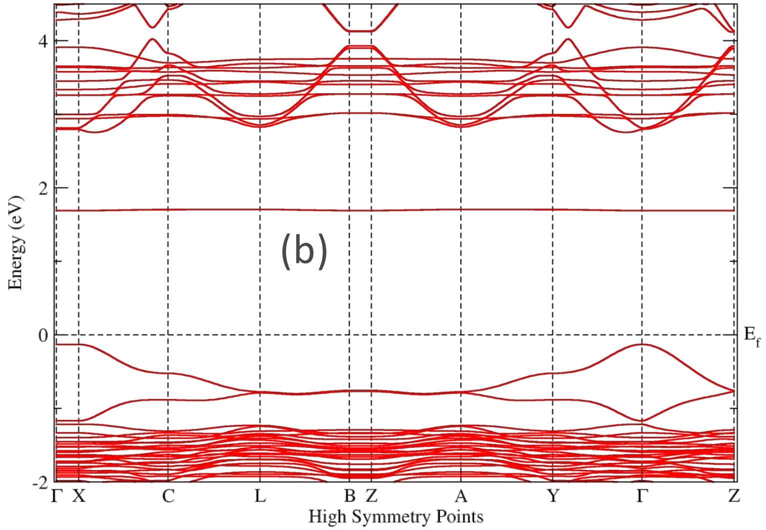

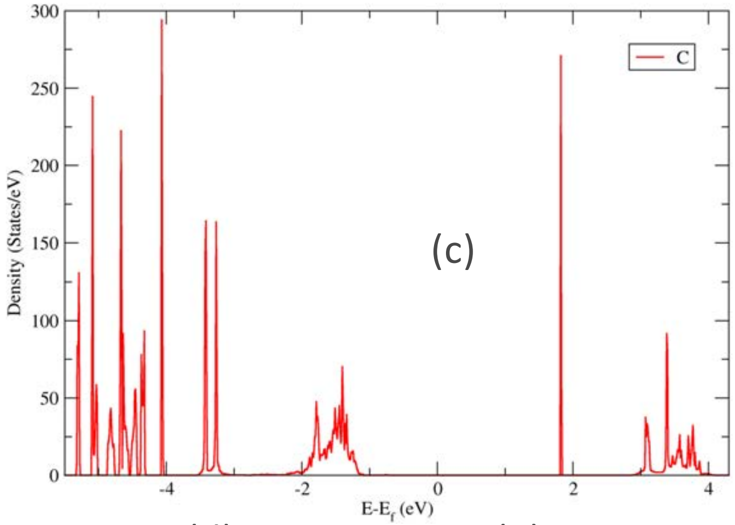

- Fig. (a) represents the monolayer crystal structure
- Fig. (b), (c), (d), and (e) show the DFT results: band, atom-resolved density of states on C-atom, charge densities (CD) of Pb-s and C-p orbitals resp. calculated using VASP
- Results identify the presence of optically inactive surface state in monolayer slab, which are attributed to surface C-atoms p-orbitals that are separated by a large distance (> 10 Å) in real space and do not overlap with Pb-s/p states forming the valence bands resulting in the absence of an optical signal in the linear regime

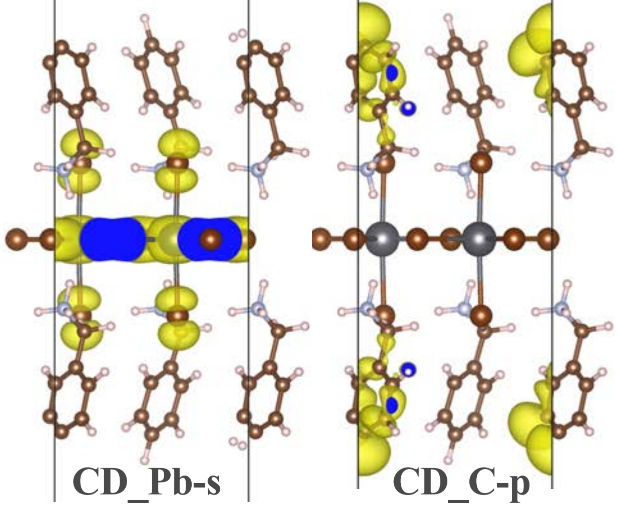

MonArk Quantum Foundry

Himal Oli

Reflectance lab set up and optical microscope images

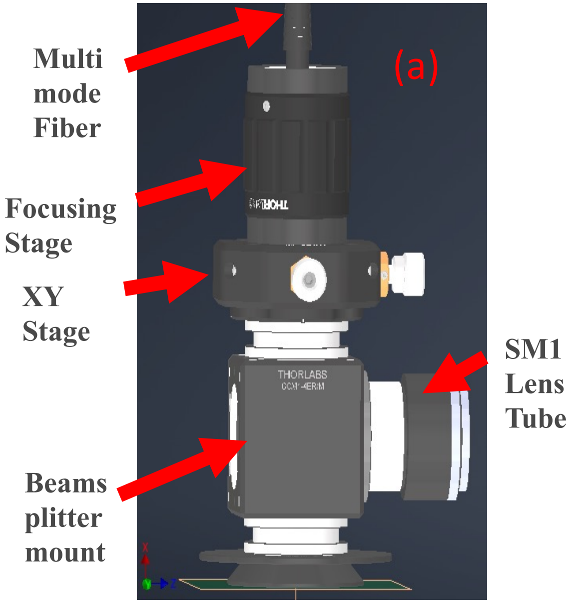

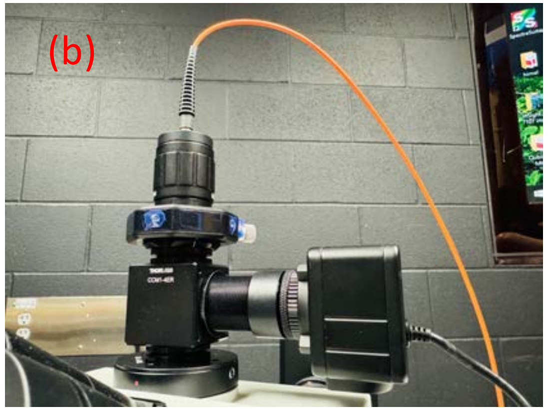

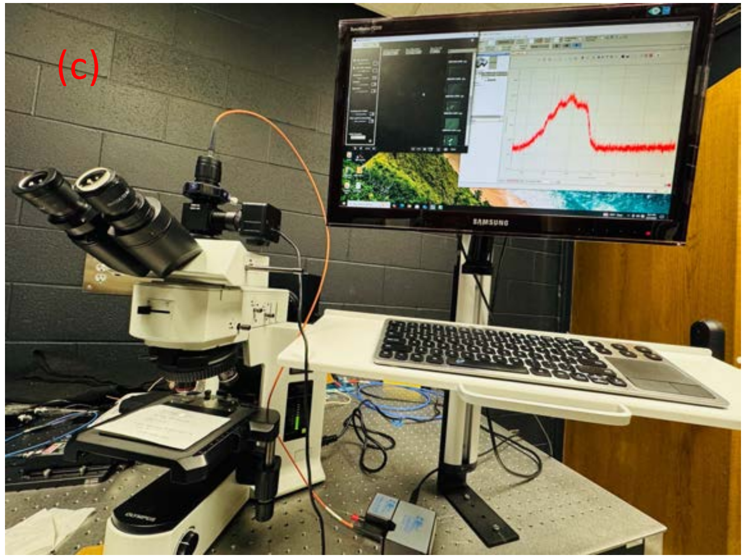

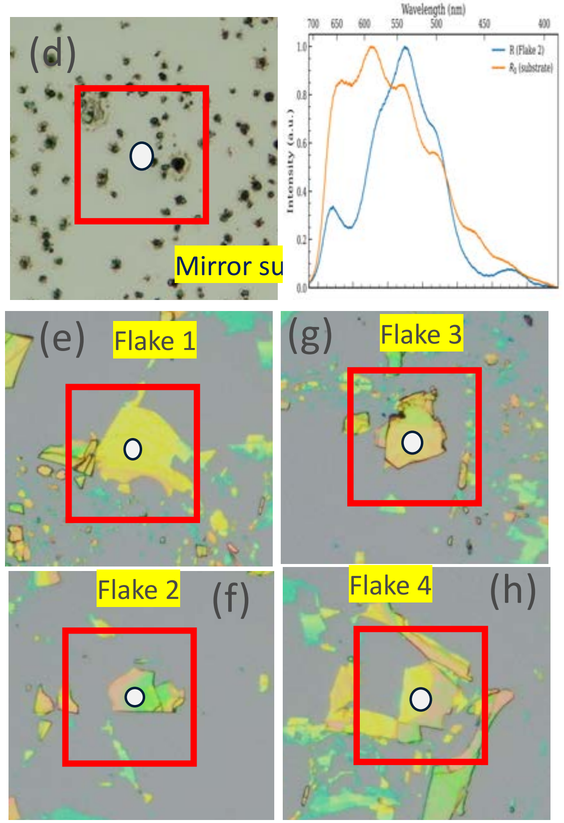

- Fig. (a), (b), and (c) represent setup designed in Autodesk Inventor, setup after assembling the parts, and the overall experimental lab setup respectively
- Fig. (d) represents the optical microscope image of mirror substrate
- Fig. (e), (f), (g), and (h) represent the mechanically exfoliated optical microscope image of different flakes of 2D $(\boldsymbol{Benzylammonium})_2\ \boldsymbol{PbBr_4}$ perovskite

SHG in 2D$(Benzylammonium)_2PbBr_4$ Perovskite

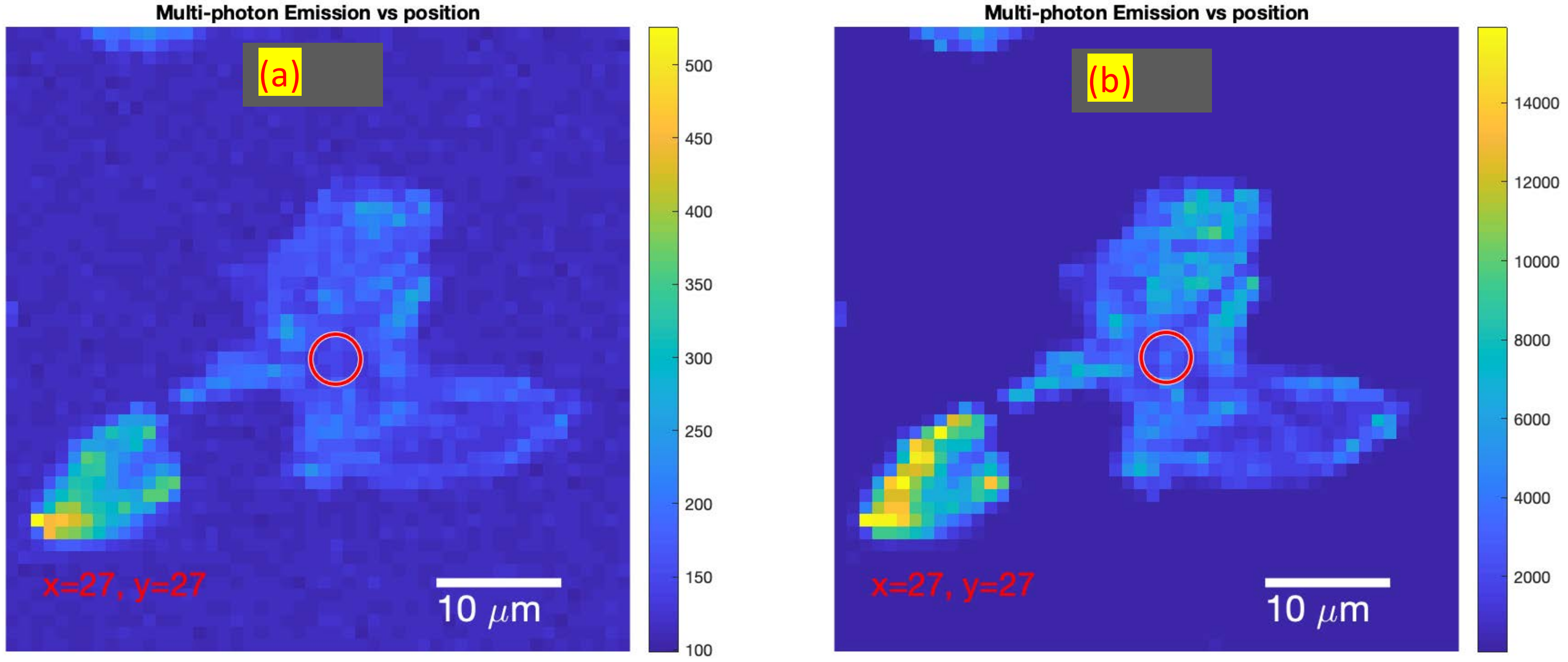

- Fig. (a) and (b) display a map of multi-photon emission vs position with & without grating respectively. It shows the spatial distribution of multi-photon emissions within the sample.

Tri-layer WSe_2 device fabricated at MonArk

MonArk
Quantum Foundry

a

Arik Ahmed

Schematic of device

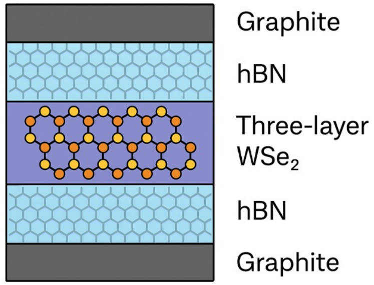

Sample holder

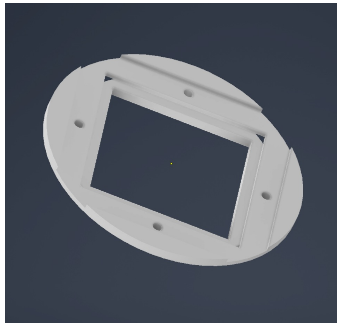

b

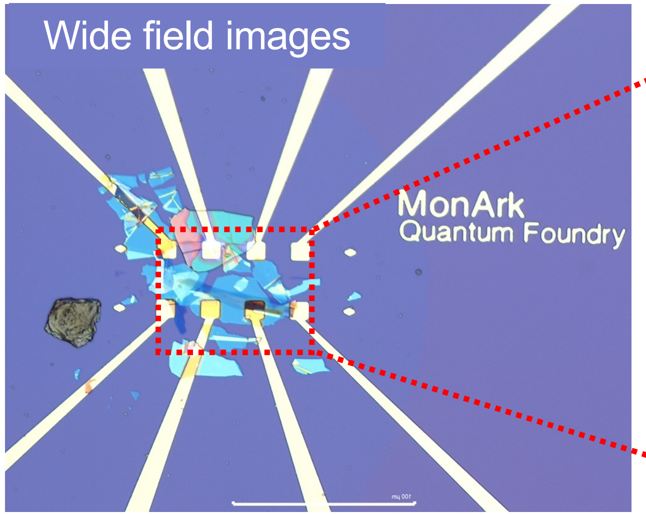

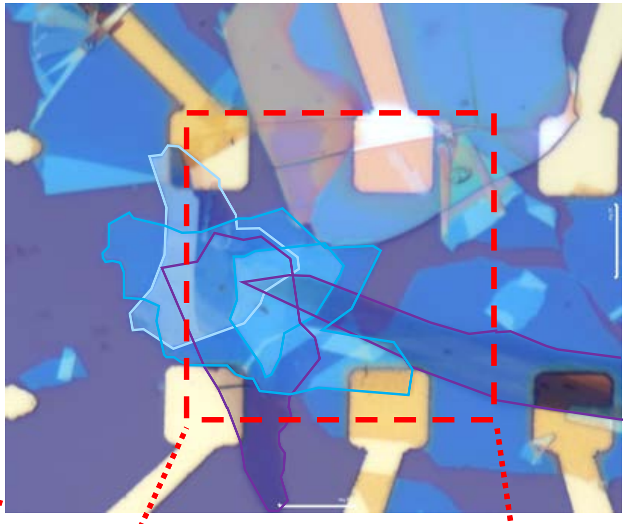

Multiphoton spectra

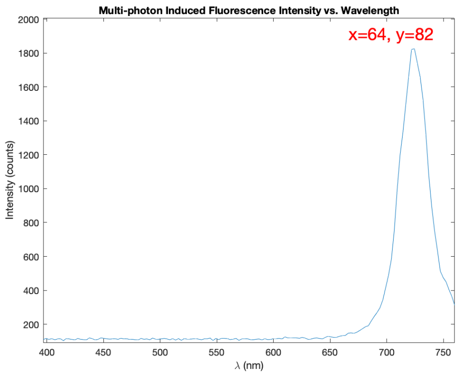

SHG image

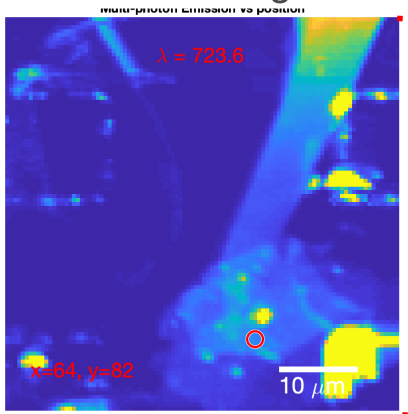

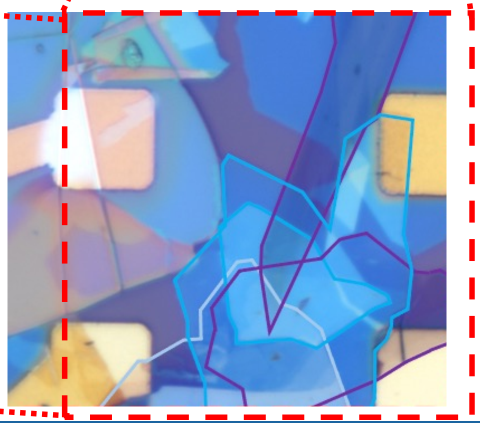

Twist angle in MoS2/WSe_2 heterojunction device (Behura)

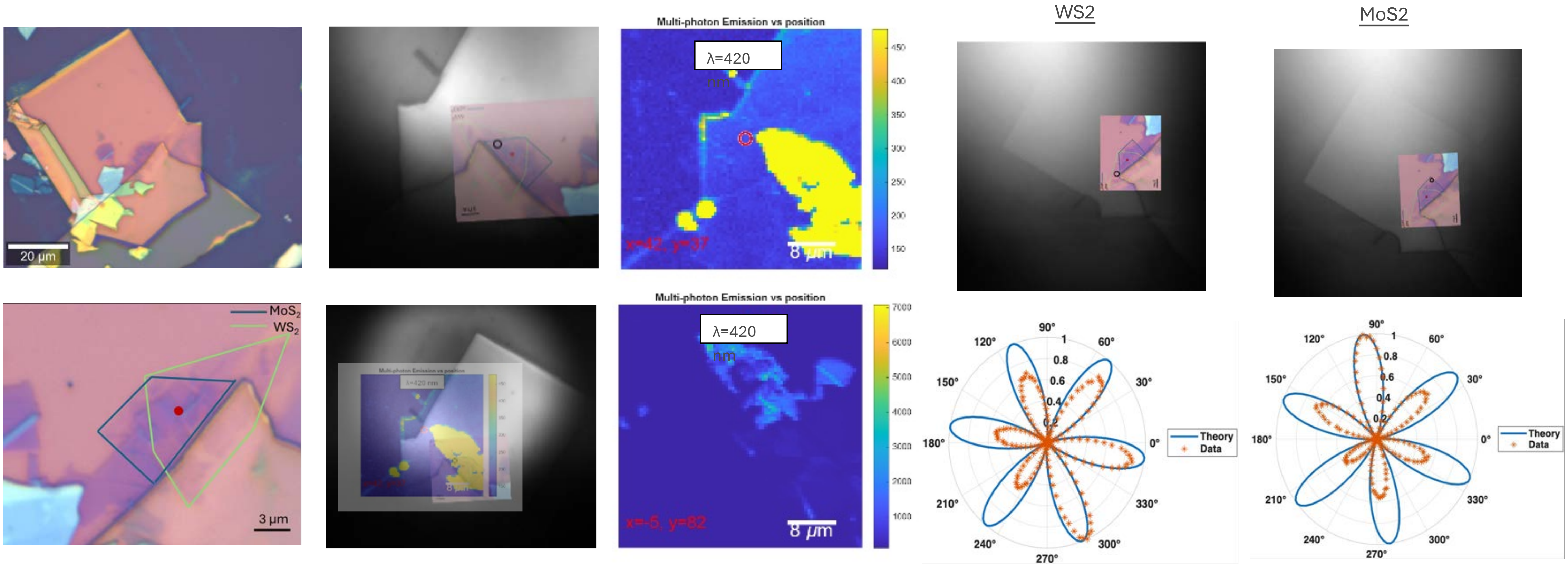

→ SHG spectroscopy on the MoS_2-WS_2 sample to determine twist angle between the MoS_2/WSe_2 bilayer

Self-assembled metasurfaces and Robotic Chemistry

Shan Zhou (2022)

MonArk Quantum Foundry

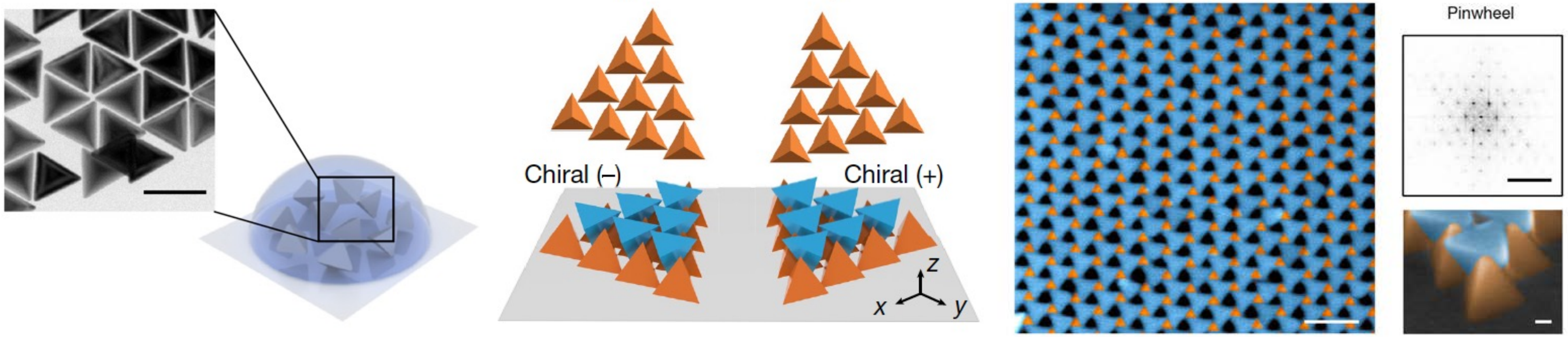

Left to right: Colloidal self-assembled tetrahedra, chiral assembly via enatiomeric coupling and SEM image of chiral metasurface.

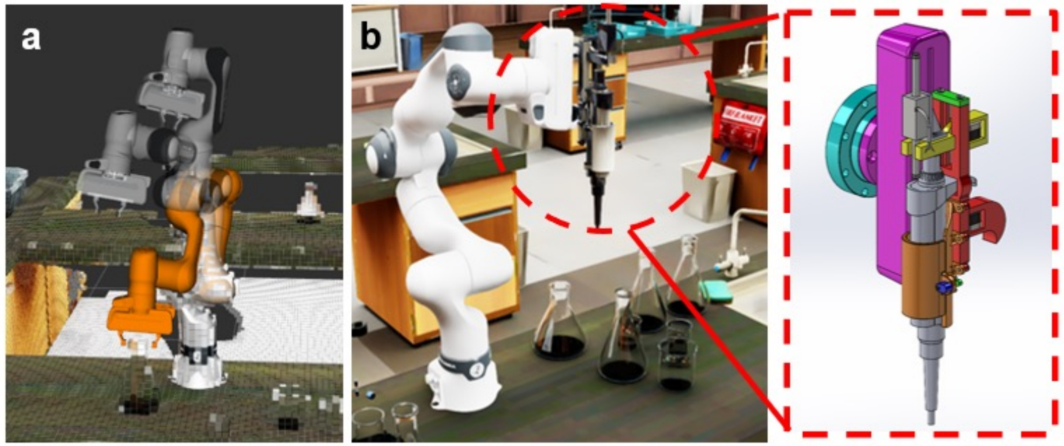

Left to right: Simulation of robotic arm, photo of arm learning chemistry and SEM CAD rendering of custom pipette actuator.

Infrastructure Improvements

MonArk Quantum Foundry

9 Tesla Cryogen Free (2025)
Physical Property Measurement System

Nano-Frazor Photothermal nano-Lithography (2025)

TEM MRI (2025)

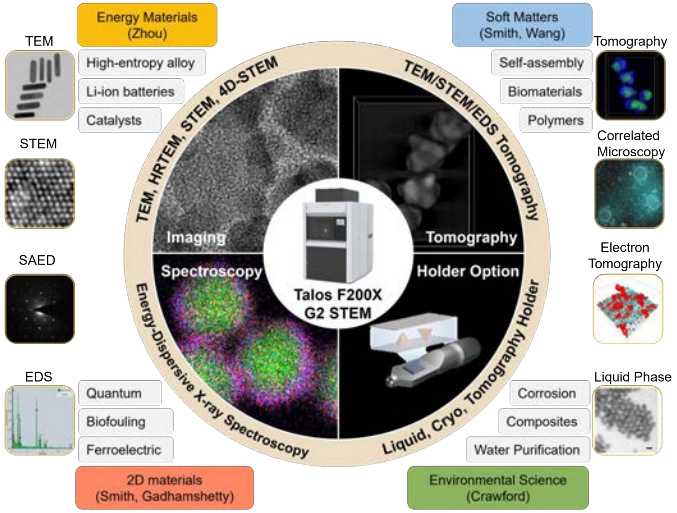

Quantum Mechanics Laboratory Kit (2024)

Quantum Cascade Laser and Near-field Microscope (2025)

6 DOF Robotic Manipulator (2026)

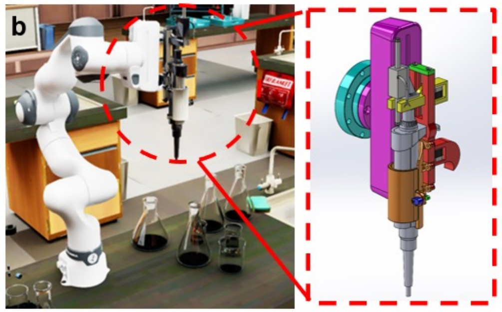

Conclusions and acknowledgements

Arik Ahmed | Himal Oli | Junming Yue | Tochukwu Emeakaroha | Kim Yip Chiok | Tolulope Ajuwon | Yoseph Loyd | Saif Bijoy

- Spatially-resolved, second harmonic and multiphoton luminescence imaged in 2D materials coupled with theory and materials synthesis.
- Ongoing investigations in a palette of 2D materials, heterostructures and metasurfaces.
- Future work will focus on heterostructures, including meta-materials.

† We acknowledge the MonArk NSF Quantum Foundry supported by the National Science Foundation Q-AMASE-i program under NSF award No. DMR-1906383, and the Quantum Materials Institute supported by the NSF Expand-QISE program under NSF award No. OSI-2427079 and our IAB members from Intel, IonQ, IBM, and CSM.